Journal of Molecular Liquids 387 (2023) 122598

Contents lists available at ScienceDirect

Journal of Molecular Liquids

journal homepage: www.elsevier.com/locate/molliq

Selective and high capacity recovery of aqueous Ag(I) by thiol functionalized mesoporous silica sorbent

Petra Herman [a], Dániel Pércsi [a,b,c], Tamás Fodor [d], Laura Juhász [e], Zoltán Dudás [c], Zsolt E. Horváth [f], Vasyl Ryukhtin [g], Ana-Maria Putz [h,*], József Kalmár [a,*], László Almásy [c,*]

[a] ELKH-DE Mechanisms of Complex Homogeneous and Heterogeneous Chemical Reactions Research Group, Department of Inorganic and Analytical Chemistry, University of Debrecen, Egyetem tér 1, Debrecen H-4032, Hungary
[b] Doctoral School of Chemistry, University of Debrecen, Egyetem tér 1, Debrecen H-4032, Hungary
[c] Institute for Energy Security and Environmental Safety, Centre for Energy Research, Konkoly-Thege Miklós út 29-33, 1121 Budapest, Hungary
[d] Institute for Nuclear Research, Bem tér 18/C, H-4026 Debrecen, Hungary
[e] Department of Solid State Physics, Institute of Physics, Faculty of Science and Technology, University of Debrecen, 4032 Debrecen, Hungary
[f] Institute for Technical Physics and Materials Science, Centre for Energy Research, Konkoly-Thege Miklós út 29-33, 1121 Budapest, Hungary
[g] Nuclear Physics Institute, ASCR, Husinec-Řež 130, 250 68 Řež, Czech Republic
[h] "Coriolan Drăgulescu" Institute of Chemistry, Bv. Mihai Viteazul, No. 24, 300223 Timisoara, Romania

ARTICLE INFO

Keywords:
Silver
Recovery
Sorption
Mesoporous silica
Surface complexation

ABSTRACT

A simplified sol–gel method was developed for the preparation of thiol functionalized porous silica particles using (3-mercaptopropyl)-trimethoxy-silane (MPTMS) for co-gelation in the presence of micellar templates. The resulting short range ordered porous silica microparticles are exceptionally effective sorbents of aqueous Ag(I). The binding of aqueous Ag(I) is almost stoichiometric in the broad pH range between 4.0 and 9.0 even at low Ag(I) concentrations until reaching the limiting 238 mg g^{-1} sorption capacity. The sorbent displays high selectivity towards Ag(I), which was tested in the simultaneous presence of several different metal compounds. The practically complete recovery of Ag(I) and the regeneration of the sorbent was achieved by washing with a 10 mM $Na_2S_2O_3$ solution. X-ray photoelectron spectroscopy (XPS) revealed that silver is not reduced on the surface of the sorbent. The reason for the strong and selective binding of Ag(I) is the formation of layered thiolate coordination compounds on the functionalized silica surface that display characteristically high stability even in the presence of other competing metal ions.

1. Introduction

Because of accelerating consumption demands, a large number of different aqueous metal compounds accumulate in various industrial waters both in the production phase and in waste management. The recovery of these metal compounds is important from an environmental point of view, and the recycling of the precious metal compounds into production is of great economic importance.

In the last decades, the industrial demand for silver and its compounds has grown rapidly, accounting for more than half of annual precious metal demand worldwide. This means that economic growth can multiply the procurement price of silver in the future, considering that, its natural abundance is limited. Due to its unique, advantageous properties, the use of silver span a wide range of technological applications and it is nearly impossible to substitute [1,2]. In industrial applications, it become an invaluable and indispensable substance, because of its resistance for corrosion, high conductivity, its sensitivity to light, as well as, its antibacterial property. The electrical and heat conductivities of silver are the highest among the elements. Because of its durability and high electrical conductivity, it is widely used for coating electrical contacts. Almost every electrical device and printed circuit board contain silver. The need for wires can be eliminated by painting silver ink on any non-metal surface serving as an electrical pathway (RFID chips). Due to the light-sensitivity of silver compounds, photography used to be a major user of it. X-ray photography is still a big consumer of silver. Besides, today the light-sensitive property of silver become essential for the photovoltaic and solar industry. Another beneficial property is its antibacterial nature, which enables its use in

* Corresponding authors.
E-mail addresses: putzanamaria@acad-icht.tm.edu.ro (A.-M. Putz), kalmar.jozsef@science.unideb.hu (J. Kalmár), almasy.laszlo@ek-cer.hu (L. Almásy).

https://doi.org/10.1016/j.molliq.2023.122598
Received 30 May 2023; Received in revised form 12 July 2023; Accepted 13 July 2023
Available online 14 July 2023

food industry, pharmacy, or even in water purification or wood preservation. Nanotechnology also uses silver particles as antimicrobial agents.

The production, use and disposal of silver and its compounds lead to the contamination of the environment, mainly the surface water [3,4]. Because of its possible toxic effect in humans (breathing problems, eye, skin, lung, throat and digestive system irritation), and its high toxicity for aquatic life, the Environmental Protection Agency (EPA) limited the concentration of silver in drinking water to 50 μg L^{-1} [5–8].

Based on these considerations, the recovery of silver is crucial from the environmental point of view, as well as to keep up with the growing industrial demand. In many cases the recovery of the precious metals has to be realized from secondary resources after treated with different reagents in selected technological steps. The resulting aqueous media usually contain high amounts of other metal (e.g. Cu, Zn, Pb, Hg, Ni) compounds. The key challenge of the immobilization of aqueous silver is its separation from these diverse media. Various methods have been reported for the recovery of dissolved silver compounds: ion exchange, precipitation, nanofiltration, reverse osmosis, sorption and membrane separation [9,10]. Among these methods, sorption stands out because of its high performance, cost effectiveness, ease of operation and quickness [11–14].

Among various kinds of sorbent materials, silica and various silica composites are widely used in large scale applications for the removal of organic and inorganic contaminants from natural and polluted waters [15–21]. The sorption capacity of porous silicas is largely dependent on the high apparent surface area, which can easily be achieved with appropriate synthesis routes [22,23]. Nevertheless, the binding ability of the SiO_2 surface is still moderate, and allows the achievement of sorption capacities in the order of 2.5–3.0 mmol g^{-1} [24–28]. The efficiency of the silica-based sorbents can be enhanced by orders of magnitude by preparing silica–carbon, or silica-organic polymer composites, or by the surface modification of the silica matrix itself. The best sorption capacities for binding Ag(I) were reported for thiourea-modified chitosan resins and for silica coated magnetic nanoparticles (>300 mg g^{-1} at pH = 5.0) [14,24].

Two main approaches exist for producing silica surfaces covered by various functional groups suited for the capture of ions or molecules from aqueous media. The more frequently used and the more sophisticated one is the modification of the surface by covalently attaching silica alkoxy molecules with various functional groups. This approach uses two or more synthesis steps. In the first step, a high specific surface silica matrix is prepared, e.g. in a sol–gel route, and subsequently, other molecules are grafted to the silica surface. The alternative way requires a single step synthesis: the functional groups are introduced in the reaction mixture together with the main silica precursor, and the material is formed in a one-pot synthesis. This is generally termed as "co-gelation" [21,29–31].

In the present work we developed a simplified one-pot route for preparing functionalized mesoporous silica particles suitable for the selective sorption of Ag(I) ions from aqueous media. The synthesis was performed at room temperature, and the conditions were varied in order to maximize the amount of active sites on the surface of the porous silica particles. The resulting family of silicas were thoroughly characterized. The thermodynamic and kinetic properties of the sorption of Ag(I) were explored under a wide range of conditions, and the mechanism of the binding of Ag(I) was investigated in details to account for the selectivity of the sorbent.

2. Experimental Section

2.1. Materials and solutions

Fine chemicals $Pd(NO_3)_2 \times 2\ H_2O$, K_2PtCl_4, $PtCl_4$, $Cu(NO_3)_2 \times 3\ H_2O$, $Cd(NO_3)_2 \times 4\ H_2O$, $Pb(NO_3)_2$, $Zn(CH_3COO)_2 \times 2\ H_2O$, $HgCl_2$, $Co(NO_3)_2 \times 6\ H_2O$, $AgNO_3$, $Ni(NO_3)_2 \times 6\ H_2O$, NaOH, hexadecyltrimethyl-ammonium bromide (CTAB), (3-mercaptopropyl)-trimethoxy-silane (MPTMS), absolute ethanol, solutions of NH_3 and HNO_3 were purchased from Sigma-Aldrich in ACS reagent grade and used without further purification. All aqueous solutions were prepared with ultrafiltered water (ρ = 18.2 MΩ cm by Milli-Q from Millipore). Tetraethyl orthosilicate (TEOS) was purchased from Fluka. A Metrohm 888 Titrando automatic titrator unit equipped with a double-junction 6.0255.100 pH electrode with KNO_3 outer electrolyte was used to measure the pH of the solutions. Common single junction electrodes containing KCl electrolyte could not be used, because of the reaction of the metal ions with Cl^-. The desired pH was set by adding HNO_3 or NaOH solutions.

2.2. Synthesis of mercaptopropyl functionalized mesoporous silicas

Mesoporous silica particles with different degrees of mercaptopropyl functionalization were synthesized by the sol–gel method using hexadecyltrimethyl-ammonium bromide (CTAB) micelles as a template. The present recipe is similar to those used for preparing MCM-41 types of materials. First, an aqueous colloid dispersion was prepared by mixing 2.00 g CTAB in 385 mL of water under continuous stirring. Next, 136 mL of ethanol and 46.4 mL of 25 wt% ammonia was added to the system and stirred for 30 min. Finally, the mixture of silica precursors was added slowly into the colloid suspension. The ratio of the different precursors was varied, as given in Table 1. The resulting reaction mixture was agitated for 3 h at room temperature. The resulting gel was collected by filtration, washed by water until constant pH, and dried at room temperature for 24 h. The CTAB template was removed by the acidic extraction method. The particles were stirred in 100 mL acidified ethanol (1.0 mL cc. HCl and 99 mL ethanol) for 2 h, and centrifuged. This step was performed 3 times. After extraction, the samples were washed with 50 mL ethanol two times and dried at 90 °C for 12 h. The complete removal of CTAB was verified by FT-IR measurements, as discussed later.

Four functionalized mesoporous silicas were produced by this recipe where 4, 7, 11 or 15n/n% of the TEOS silica precursor is substituted by MPTMS. The parent silica was prepared by the same recipe using only TEOS (Table 1). The as-prepared functionalized mesoporous silicas are referred to simply as"***xerogels***" in the text onward.

2.3. Xerogel characterization

The samples were imaged using a ThermoFisher Scientific Scios 2 dual beam scanning electron microscope (SEM). The unique in-lens detector system and the retarding-field option enabled the low voltage scanning electron microscopy (LV-SEM) imaging of the pristine xerogel samples without applying any conductive coating. Typically, an acceleration voltage of 1–2 kV and 2–5 mm working distance was used. The freshly fractured xerogels were fixed on vacuum-resistant carbon tapes. The microscope is equipped with a removable Bruker QUANTAX energy dispersive X-ray spectroscopy (EDS) detector (Billerica, Massachusetts, USA). For the EDS analysis, an accelerating voltage of 15 kV was used and a long measure time was applied to improve the signal/noise ratio.

Transmission electron microscope (TEM) images were obtained using a JEOL 200 FX-II TEM instrument. The powdered xerogel samples were sonicated in ethanol for 10 min, after which the dilute suspension was dropped onto a TEM grid covered with carbon.

Table 1
The reagents used for the preparation of the (functionalized) mesoporous silicas.

	CTAB (g)	TEOS (mmol)	MPTMS (mmol)	MPTMS content (n/n%)
SH0	2.0	36	–	–
SH4	2.0	35	1.4	4.0
SH7	2.0	34	2.7	7.0
SH11	2.0	33	4.0	11
SH15	2.0	36	5.4	15

Nitrogen adsorption–desorption porosimetry was performed in a Quantachrome Nova 2200e instrument. The xerogels were degassed at 60 °C for 24 h. The multipoint BET method was used to calculate the apparent surface area based on 5 points on the adsorption curve (maximum $p/p_0 = 0.30$). Pore size distribution was calculated based on the desorption curve using the NL-DFT method for amorphous silica surfaces.

Powder X-ray diffraction (XRD) was performed on a Bruker AXS D8 Discover diffractometer equipped with a Göbel mirror and a scintillation detector using Cu Kα radiation. Measurements were performed over the interval 2–8° with a step size of 0.04° and a scan speed of 0.10°/min. The materials were placed on double-sided adhesive tapes.

The **infrared spectra (IR)** of the pristine xerogel samples were recorded by a PerkinElmer Spectrum Two FT-IR instrument. The instrument is equipped with a universal ATR head (Attenuated Total Reflectance – Single Reflection Diamond – L1600607) enabling the direct analysis of solid samples. The IR spectra were recorded in the range of 450–4000 cm^{-1} at 55–95 % transmittance.

The **size distribution** of the xerogel particles was measured after grinding the samples in the appropriate aqueous media by a Potter-Elvehjem tissue grinder (5 min) followed by sonication (15 min). Light microscopy images were taken on the suspensions ($c_{Xgel} = 0.50$ g/L) in a hemocytometer with a 1.3 MP USB camera. The ImageJ software was used for calculating the size distribution of the particles.

The **Zeta potential** of the dispersed xerogel particles ($c_{Xgel} = 0.50$ g/L) was measured in a MALVERN Zetasizer Nano ZS instrument using conventional experimental setup and instrument operation. The lower pH limit of the measurements is pH = 3.0. Zeta potentials were calculated using the instrument controlling software.

Small-angle neutron scattering (SANS) technique was used to reveal the overall morphology of the nanoparticles in the size range 100 nm–1 μm. SANS measurements were conducted at the double-bent crystal SANS instrument MAUD operating at the thermal channel of the LVR15 10 MW research reactor in Řež, Czech Republic [32]. The model of spherical particles with the log-normal distribution of sizes was used to fit the experimental data. The fitting was performed using the SASprofit software.

2.4. Batch sorption experiments

The sorption properties of the suspended xerogels were tested using several metal ions in batch sorption experiments at constant pH, as detailed in the Supporting Information. Xerogel suspensions were prepared by wet grinding. Metal ion solutions were mixed with xerogel suspension and stirred for an equilibration period. The supernatant was separated from the sorbent by centrifugation, and the metal ion concentrations of the two phases were measured following sample preparation using inductively coupled plasma optical emission spectrometry (ICP-OES), as detailed in Section 2.9 and in the Supporting Information.

It was proved by independent experiments that the pH of a heterogeneous sample is constant during the batch sorption experiment. The maximum difference between the initial pH and the final pH in the separated supernatant was less than 0.13.

2.5. Selectivity of xerogel sorbent

The selectivity of the xerogels was tested in the simultaneous presence of aqueous Ag(I), Cd(II), Co(II), Cu(II), Zn(II), Pb(II), Hg(II) and Ni(II) ions at pH = 5.0. Another set of experiments was carried out to test the selectivity in the simultaneous presence of aqueous Ag(I), Pt(II), Pt(IV) and Pd(II) at pH = 2.0. The initial concentrations of the metal ions were varied between $c_0 = 10$ to 200 mg/L.

2.6. Hydrolysis of metal ions

The possibility of the spontaneous hydrolysis and precipitation of the metal ions was investigated in details as given in the Supporting Information. The aqueous species distribution of Ag(I) is given in Section 3.2.3.

2.7. Time-resolved experiments, kinetics of sorption

In order to study the rate at which the sorption equilibrium is reached, time resolved experiments were carried out at $c_0 = 50$ mg L^{-1} metal ion concentrations at pH = 5.0. The same protocol was used as in case of the batch experiments, but the length of the contact time was varied between 5 min and 4 h under agitation.

2.8. Recovery of Ag(I), sorbent regeneration

The recovery of Ag(I) and the reversibility of its binding was tested by washing the previously equilibrated xerogels with EDTA (5 mM, pH = 5.0), NH_3 (5 mM) and $Na_2S_2O_3$ (10 mM, pH = 5.0) solutions in separate experiments. The same experimental protocol was applied as in the sorption experiments. After centrifuging the equilibrium mixture of the xerogel and the Ag(I) solution, the supernatant was quantitatively decanted and analysed for Ag(I). Subsequently, 8.00 mL of regenerating solution was added to the leftover xerogel pellet at a pre-set pH. The xerogel was suspended, agitated for 1 h and centrifuged for a second time. The pellet and the supernatant were separated and analyzed. The regenerated xerogel was re-suspended in 8.00 mL dilute HNO_3 solution (pH = 5.0) to remove any traces of leftover washing liquid. The system was centrifuged again and the supernatant was discharged. The regenerated xerogel was suspended in 4.00 mL dilute HNO_3 solution (pH = 5.0) and tested again for Ag(I) sorption. Altogether, three sorption-regeneration cycles were performed with one individual sample of xerogel.

2.9. Elemental analysis by ICP-OES

The metal ion contents of supernatants and washing liquids and digested pellets were measured using ICP-OES. The methods of sample preparation and the measurement conditions are given in details in the Supporting Information.

2.10. X-ray photoelectron spectroscopy (XPS)

Samples were freshly ground in an agate mortar, glued to copper sample holders with double-sided adhesive tapes and left to degas in the high vacuum of the sample loading chamber (10^{-7} mbar) overnight. The measurements were performed using an XR 50 dual-anode non-monochromatized X-ray source and a Phoibos 100 MCD-5 hemispherical energy analyzer by SPECS (Berlin, Germany). The base vacuum in the instrument was 5×10^{-10} mbar. Spectra were recorded with Al Kα radiation (1486.6 eV) at 10 kV acceleration voltage and 10 mA emission current. The energy scale was calibrated with the Au 4f7/2 (89.98 eV) and Cu 2p3/2 (932.67 eV) lines of a freshly sputter-cleaned sample containing both metals, as prescribed by the manufacturer. Charge referencing was performed with the Si 2p peak of silica (103.5 eV) of the xerogels. The spectra were processed with the CasaXPS software, and the Ag 3d peaks were fitted with Gauss-Lorentz curves using Shirley backgrounds.

3. Results

3.1. Characterization of the mesoporous silica sorbents

3.1.1. Electron microscopy

Representative SEM and TEM images of the as-prepared mesoporous silicas are shown in Fig. 1. The bulk of the xerogels are built from spherical nanoparticles (globules). The size of these globules is in the range of $d_{globule}$ = 150–200 nm. Only a short-range order of the

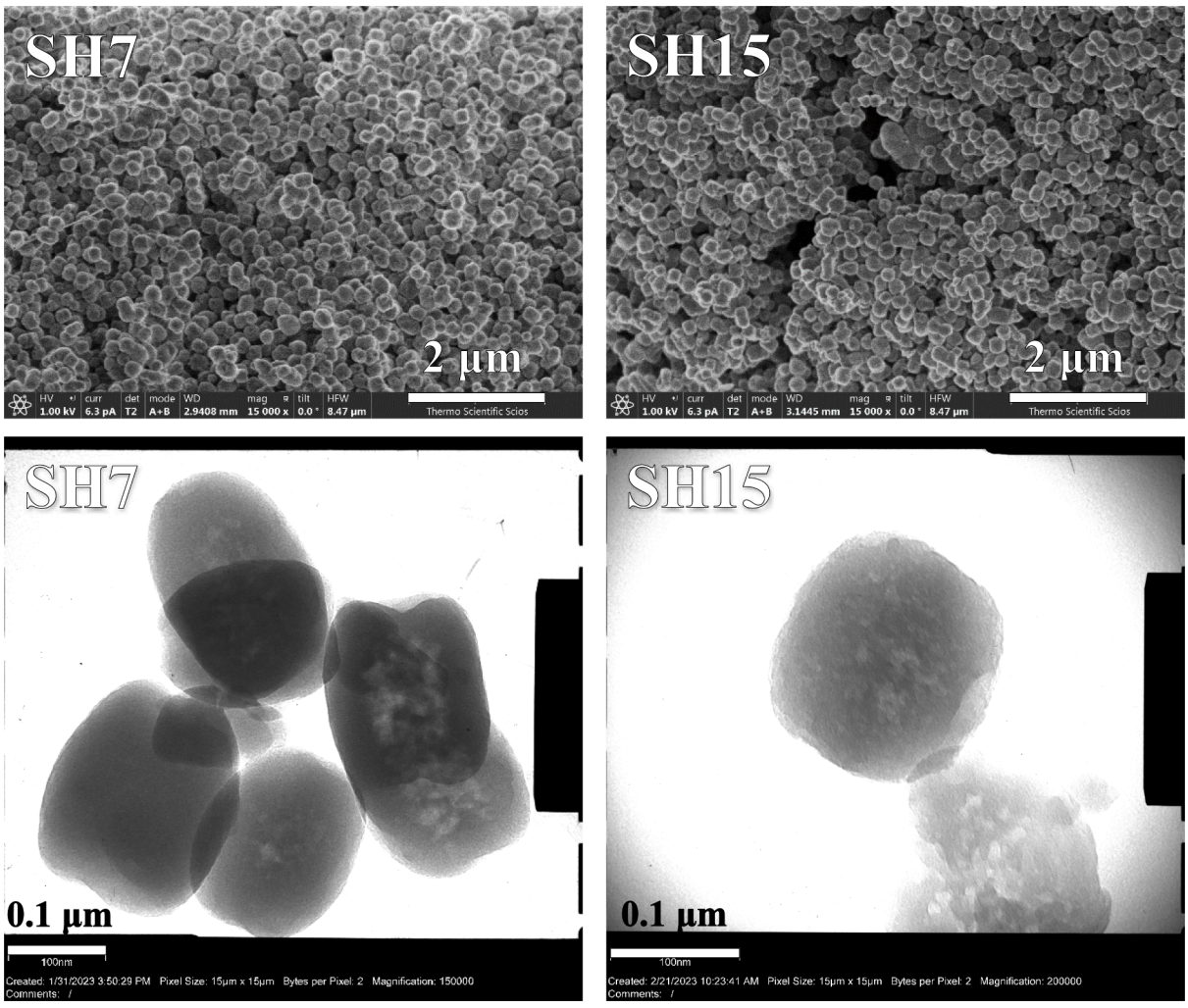

Fig. 1. LV-SEM and TEM images of the as-prepared mesoporous silicas.

mesoporosity is visible in the TEM images, which is in good accordance with the N_2-sorption and the XRD data, as discussed in the next sections. This is in contrast with the characteristics of the MCM-41 type materials that display long range ordered mesoporosity. The introduction of the mercaptopropyl functionalized silica precursor (MPTMS) resulted in the slight increase of the sizes of the globules, however, significant morphological changes are not seen on the SEM and TEM images. The morphology of the particle agglomerates were studied further by ultra-small angle neutron scattering (SANS), as discussed in the Supporting Information. The pore structure of the particles was investigated using N_2-sorption porosimetry, as follows.

3.1.2. *Nitrogen-sorption porosimetry*

The experimental N_2-sorption isotherms and the calculated pore size

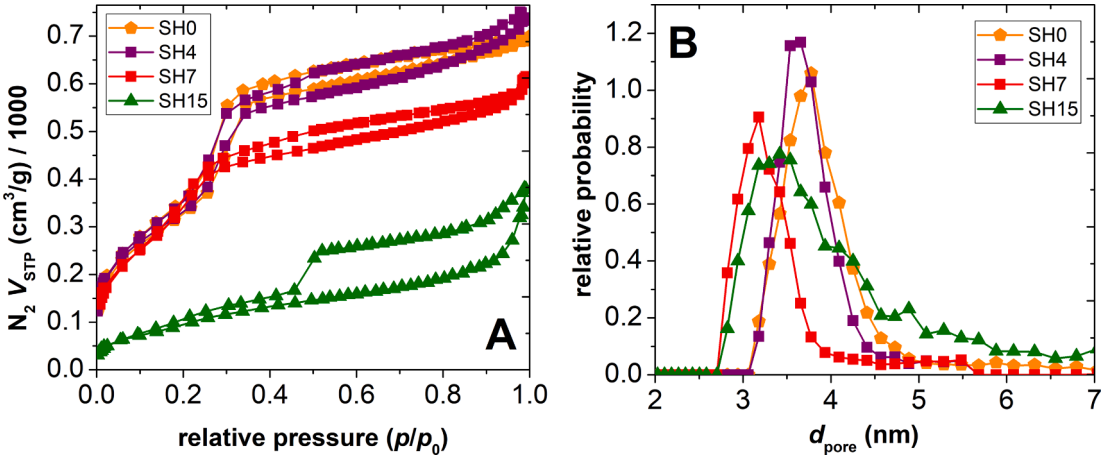

Fig. 2. N_2-sorption isotherms (A) and pore size distributions calculated by NL-DFT (B).

distributions are shown in Fig. 2. The estimated structural parameters are collected in Table 2. Based on the IUPAC classification, the majority of the isotherms are type IVb, which is characteristic for mesoporous materials with conical and cylindrical pores. The only exception is the SH15 xerogel where the isotherm is type IVa with an H2b hysteresis loop. This is characteristic for mesoporous materials with a narrow size distribution of pores with wide necks [33]. The structural modification effect of the increasing quantity of the mercaptopropyl functionalization can be observed on the change of the shape of the hysteresis loop. The highest functionalization degree resulted in the lowest apparent surface area in the case of the SH15. Furthermore, the alteration of the shape of the hysteresis loop indicates that the dominant porosity changed from conical and cylindrical type pores to ink bottle type pores. This is also observed in the XRD experiments and in the electron microscopy pictures to some extent.

3.1.3. X-ray diffraction

The XRD data for the five mesoporous silica samples are shown in Fig. 3. They display the low angle reflections characteristic to the hexagonally ordered channels of the MCM-41 type ordered mesoporous silicas. All samples display a strong diffraction peak at 2 theta angles between 2 and 2.5°, corresponding to the mean interpore distances. The position of the peak shifts towards the larger angles with increasing MPTMS content, as marked in the inset, showing the gradual decrease of the interpore spacing, in agreement with the decrease of the pore sizes observed by the N_2-sorption. The higher order diffraction peaks (1 1 0) and (2 0 0) are vaguely visible in the patterns, indicating the relatively poor long range order. The ordered mesoporous structure is further corroborated by the TEM images and shapes of the N_2-sorption hysteresis loops. Overall, all of these characterization data are aligned in the sense that they show a short range ordered mesoporous structure for the present mercaptopropyl-functionalized silicas, in contrast to the long range ordered pore structure of the MCM-41 silicas. Furthermore, the pore structures of the present silicas are altered by the variation of the MPTMS content of the synthesis mixture, and thus, the functional group content of the final materials.

3.1.4. Infrared spectroscopy

All xerogels show the main specific vibration bands of the silica skeleton at 1050, 800 and 450 cm^{-1} (Fig. 4). They are assigned to the asymmetric stretching, symmetric stretching and bending vibrations of the Si—O—Si network, respectively [34]. Likewise, all xerogels show the characteristic bands for the O—H groups, as follows. The broad band around 3300 cm^{-1} corresponds to the overlapping of the O—H stretching bands of hydrogen-bonded water molecules and the Si—O—H stretching of the surface silanols hydrogen-bonded to water [35]. The bands around 3740 cm^{-1} indicate a large amount of free silanols on the silica surface [36]. The bands around 1640 cm^{-1} correspond to vibrations of water and to those of the SiO_2 network, as well [36]. The C—H vibrations of the alkyl chains of any remaining CTAB were expected to show bands around 2900 cm^{-1}. The absence of these bands verify the complete removal of the surfactant from the xerogels [37].

The characteristic, but weak S—H stretching vibration bands, expected around 2560 cm^{-1} could not be detected, because of their low intensities [31,38,39]. However, the C—S vibration band at around 700 cm^{-1}, and the C—H scissoring vibration bands around 1480 cm^{-1} visible in the functionalized xerogels indicate the presence of the mercaptopropyl groups covalently bound to the silica matrix (following the complete removal of the surfactant) [40].

Table 2
Structural parameters estimated from the N_2-sorption isotherms shown in Fig. 2.

Sample	BJH		DFT (nm)	Apparent surface area (m^2/g)	Total pore volume (cm^3/g)
	Ads (nm)	Des (nm)			
SH0	3.2	3.2	3.8	1256	1.02
SH4	3.2	3.5	3.7	1237	1.01
SH7	3.2	3.2	3.2	1106	0.81
SH15	3.2	3.9	3.4	398	0.34

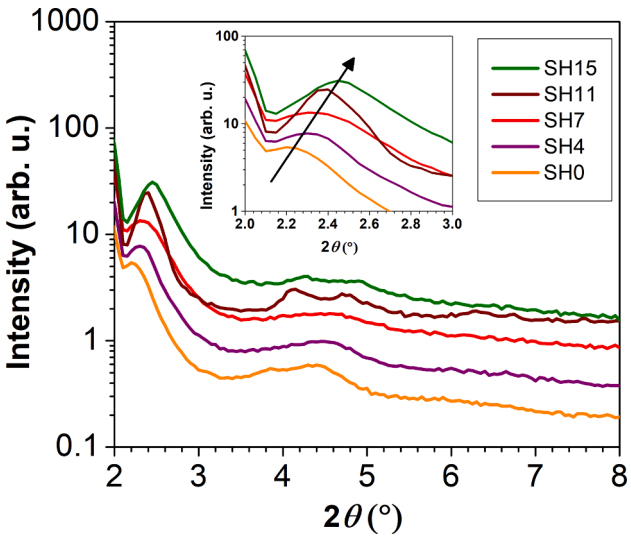

Fig. 3. X-ray diffractograms of the functionalized mesoporous silicas.

3.1.5. Size and Zeta potential of hydrated xerogels particles

The as-prepared silica powders spontaneously disintegrate in water yielding micrometer sized particles. After wet grinding the suspended xerogel using a standardized protocol, the particle size distribution was measured in the suspension. The xerogels show a narrow size distribution with ca. 5 μm mean size of the hydrated particles (Fig. 5).

The Zeta potentials of the suspended xerogel particles were measured in the pH range from 3.0 to 9.0 (Fig. 5). The SH0 and SH7 particles have approximately the same Zeta potentials of ca. +55 mV and +50 mV, respectively, at pH = 3.0. In the case of the SH0 particles, the Zeta potential steeply decreases after pH = 4.0 with the isoelectric point being between pH = 4.0–5.5, which is characteristic to amorphous silica materials [41]. The incorporation of the mercaptopropyl groups increases the basicity of the silicas, which is reflected in the pH dependence of the Zeta potentials of the functionalized samples. The Zeta potential of the SH7 sample starts decreasing only above pH = 7.0. Until this point the Zeta potential of the functionalized silica is highly positive and the isoelectric point of the suspended functionalized xerogel is ca. pH = 8.7.

3.2. Sorption of aqueous Ag(I)

3.2.1. Selectivity of the sorbents

The affinity of the xerogels were tested towards Ag(I), Cd(II), Co(II), Co(II), Hg(II), Ni(II), Pb(II), Zn(II) at pH = 5.0 in batch sorption experiments. The sorption of metal ions was studied individually, and also in the simultaneous presence of multiple metal ions. All of the batch sorption experiments consistently show that the xerogels have unprecedentedly high selectivity for binding Ag(I). The amounts of metal ions sorbed by SH15 at pH = 5.0 at c_0 = 50 mg L^{-1} initial metal ion concentration are shown in Fig. 6. Besides Ag(I), none of the metal ions show significant affinity to bind to the xerogels.

Independent sorption measurements were carried out to test the affinity of the xerogels towards Pd(II), Pt(II), Pt(IV). Considering the solubility of aqueous Pd(II) (100 mg L^{-1} at pH = 2.5), these experiments were performed at pH = 2.0. As shown in Fig. 6, these precious metal ions showed only a minor affinity towards the mercaptopropyl functionalized xerogels, which is negligible compared to the sorption of Ag (I).

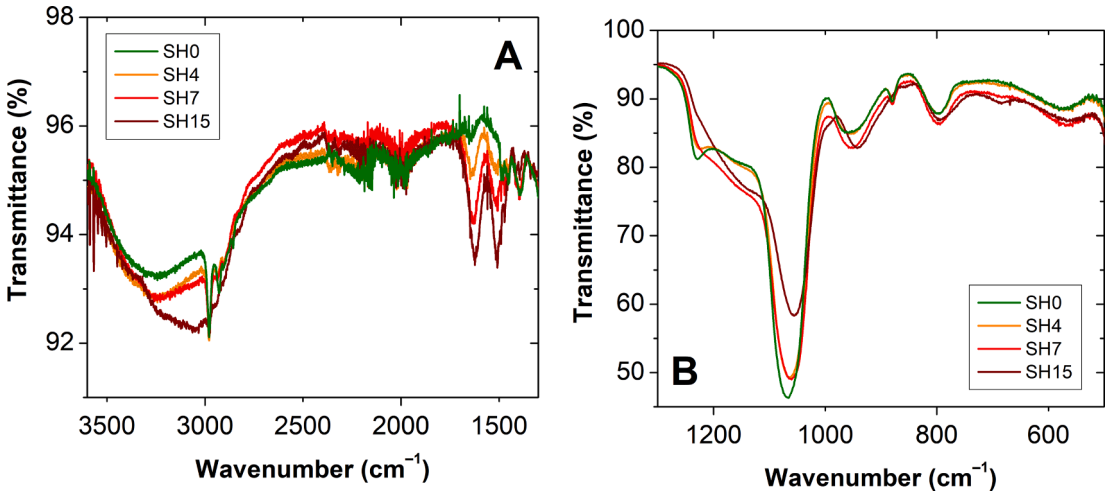

Fig. 4. FT-IR spectra of the as-prepared (functionalized) mesoporous silicas.

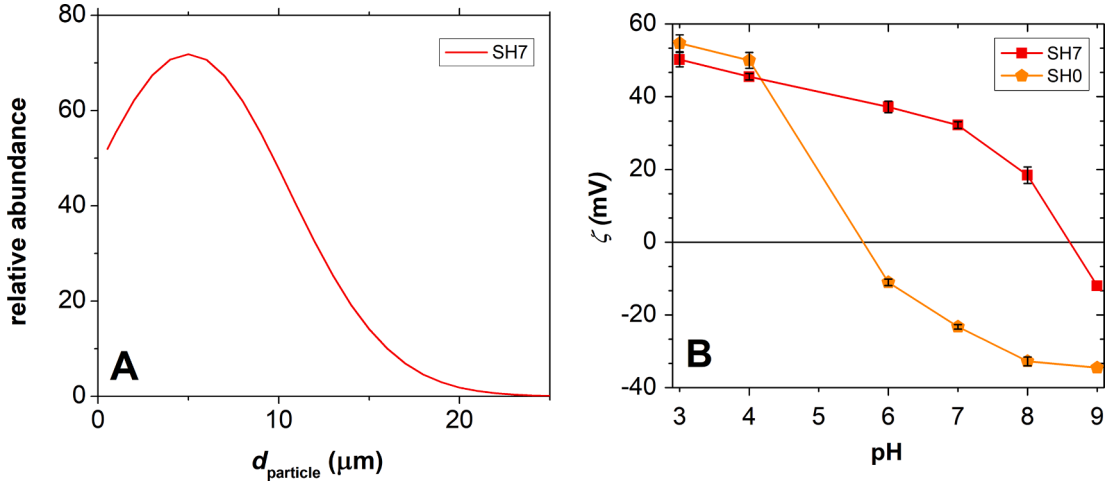

Fig. 5. Particle size distribution (A) and Zeta potential (B) of the hydrated mesoporous silica microparticles.

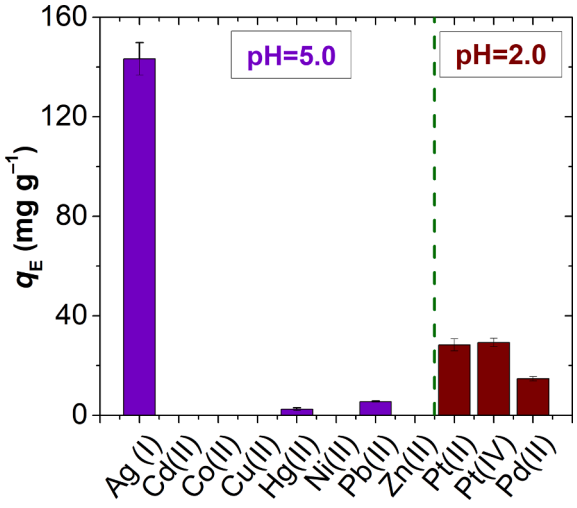

Fig. 6. Amounts of metal ions sorbed by SH15 at pH = 5.0 and at pH = 2.0 measured in the simultaneous presence of multiple metal ions ($c_{0\ M}$ = 50 mg L^{-1}; c_{Xgel} = 320 mg L^{-1}, T = 25 °C).

3.2.2. *Sorption isotherms*

Sorption isotherms were measured using different initial Ag(I) concentrations (c_0Ag(I) between 10 and 200 mg L^{-1}). The experimental isotherms evidently show that the sorption capacity markedly increases with the increasing mercaptopropyl content of the xerogels, indicating that these functional groups provide the active sites for Ag(I) binding (Fig. 7).

In order to quantify the sorption equilibria, the data points were fitted with an adequate isotherm model. Based on the experimental data, the interaction between the sorbent and Ag(I) is strong and specific. The binding is practically stoichiometric as no Ag(I) remains in solution until the complete saturation of the active sites. The effect of pH also confirmed the strong coordination of Ag(I) to the functionalized xerogels, because the sorption capacity is practically independent from the pH in the range of pH = 5.0–9.0, as detailed in Section 3.2.3.

Based on the above considerations, the sorption capacities of the xerogels were estimated using the simplest equilibrium model assuming equivalent binding sites, i.e. the Langmuir model. The Langmuir model does not specify the physico-chemical mechanism of the binding, but assumes the existence of a dynamic equilibrium. The effect of the competitive reactions of Ag(I) in the aqueous phase (e.g. hydrolysis, complexation) can be neglected at constant pH, because the speciation of aqueous Ag(I) is independent of its final concentration in the solution. In view of all these considerations, the Langmuir model is suitable for

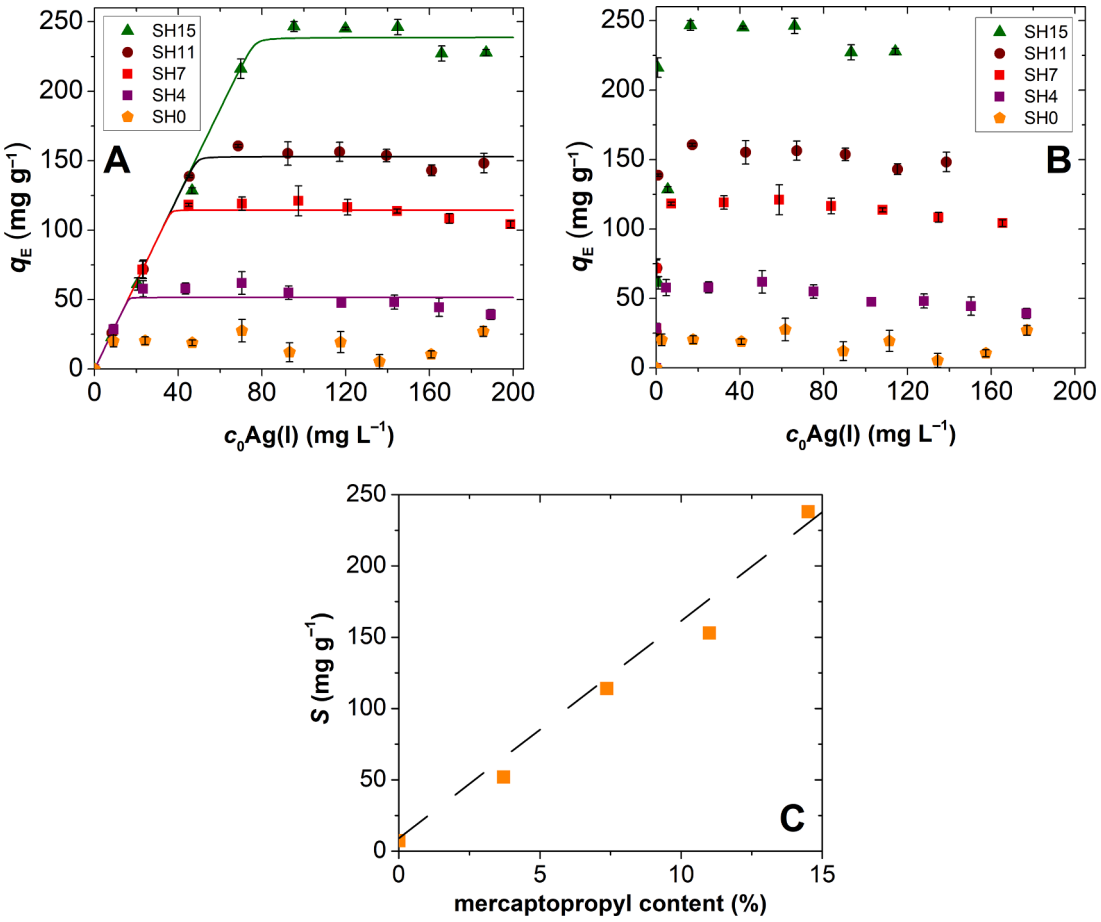

Fig. 7. Panels A and B: Sorption isotherms of Ag(I) on the xerogels at pH = 5.0 either showing the initial aqueous Ag(I) concentrations (panel A) or the equilibrium aqueous Ag(I) concentrations (panel B) on the *x*-axis. Symbols: experimental data points. Lines: nonlinear least squares fits using the Langmuir isotherm model (eq. (1). The estimated isotherms parameters are summarized in Table 3. (c_{Xgel} = 320 mg L^{-1}; c_0Ag(I) = 10–200 mg L^{-1}; T = 25 °C). Panel C: The sorption capacities of the xerogels as a function of their mercaptopropyl contents estimated by fitting with the Langmuir model.

the formal description of Ag(I) sorption under the applied conditions at constant pH. (Naturally, the interactions affecting the binding of aqueous Ag(I) are regulated by the pH, which is discussed in details in Section 3.2.3.) The mathematical equations of the Langmuir isotherm, using the equilibrium or the initial Ag(I) concentration, are as follows:

$$q_E = \frac{[Ag(I)]_{ads}}{c_{Xgel}} = \frac{K_L[Ag(I)]_{sol}S}{1 + K_L[Ag(I)]_{sol}} \quad (1)$$

$$q_E = \frac{[Ag(I)]_{ads}}{c_{Xgel}} = \frac{\left\{\left(c_{Xgel}S + c_{Ag(I)} + \frac{1}{K_L}\right) - \sqrt{\left(c_{Xgel}S + c_{Ag(I)} + \frac{1}{K_L}\right)^2 - 4c_{Ag(I)}c_{Xgel}S}\right\}}{2c_{Xgel}}$$

Here, q_E is the amount of metal ion sorbed on equilibrium per unit weight of sorbent, (mg g^{-1}), $[Ag(I)]_{ads}$ is the solution-equivalent concentration of sorbed Ag(I) at equilibrium (mg L^{-1}), c_{Xgel} is the concentration of the xerogel (g L^{-1}), $[Ag(I)]_{sol}$ is the equilibrium concentration of aqueous Ag(I) (mg L^{-1}) and $c_{Ag(I)}$ is the initial Ag(I) concentration (mg L^{-1}). S is the capacity of the sorbent (mg g^{-1}) and K_L is the Langmuir equilibrium constant (L mg^{-1}).

In each case, the sorption of Ag(I) is quantitative until reaching the maximum capacity of the sorbent, meaning practically zero equilibrium aqueous Ag(I) concentrations at low initial Ag(I) concentrations (Fig. 7B). Naturally, the equilibrium constants are very large in such cases, because the processes are quasi-stoichiometric. Isotherm fitting was performed nonlinearly using the Levenberg-Marquardt least-square algorithm. In each case, the K_L value had to be set to a minimum of 100 L mg^{-1} to get a good fit, which signifies that the K_L values are very large due to the quantitative nature of the sorption. The fitted isotherms are shown in Fig. 7A and the estimated parameters are given in Table 3. It is clearly seen in Fig. 7C, that the sorption capacity increases approximately linearly with the increasing mercaptopropyl content. The maximum sorption capacity of 238 ± 4 mg g^{-1} was measured for SH15 at pH = 5.0, with an equilibrium constant of $K_L \geq 100$ L mg^{-1}. Interestingly, the sorption capacity is not influenced by the apparent surface area of the xerogels, but only by the amount of thiol groups.

3.2.3. *Effect of pH on the sorption of Ag(I)*

One of the most important factors generally affecting sorption processes is the pH. Both the hydrolysis of Ag(I), and the protonation of the functional groups of the sorbent is strongly influenced by pH.

In order to understand the mechanism of the binding of Ag(I) and to

Table 3
Isotherm parameters estimated by fitting the experimental isotherms to the Langmuir model (eq. (1). The fitted curves are displayed in Fig. 7A.

Code	Langmuir model	
	S (mg g^{-1})	K_L (L mg^{-1})
SH15	238 ± 14	≥100
SH11	153 ± 12	≥100
SH7	114 ± 12	≥100
SH4	52 ± 8	≥100

find the optimum pH for its sorption, the quantitative description of the hydrolysis of Ag(I) is essential. Fig. 8A shows the speciation of aqueous Ag(I) calculated using the published thermodynamic equilibrium constants [42]. The hydrolysis of Ag(I), i.e. the formation of hydroxo-Ag(I) and oxo-Ag(I), is significant only under basic conditions and it is complete at ca. pH = 10.0 with the formation of the charge neutral Ag_2O. As seen in Fig. 8A, the formation of AgOH and $Ag(OH)_2^-$ is negligible under the applied conditions. In independent control experiments the absence of precipitate formation was confirmed under the applied conditions (cf. Section 2.6).

The pH also has a strong effect on the protonation state of the functional groups of the sorbent. The Zeta potentials of the functionalized silicas are positive at pH = 5.0, indicating positive apparent surface charges. The spontaneous deprotonation of the –SH groups starts around pH = 8 (cf. Fig. 5). This also confirms the strong and specific interaction between the Ag(I) and the sorbent, because the coordination of Ag(I) is favored in spite of the need of the Ag(I) assisted deprotonation of the –SH functional groups for complex formation.

It was proved in independent experiments that the sorption capacity of the xerogels does not practically change as a function of pH (Fig. 8B). All functionalized silicas bind Ag(I) even under acidic conditions and the sorption isotherm is unchanged until the start of precipitation of Ag(I) above pH = 9. The strong and selective binding of Ag(I) in a wide pH range is a major advantage considering practical applications.

3.2.4. Time-resolved sorption experiments

As seen in Fig. 9, the sorption equilibrium establishes extremely fast, after 5 min of agitation (and 10 min of centrifugation). The rate of the binding of Ag(I) is practically independent of the initial Ag(I) concentration and the mercaptopropyl content of the xerogel (Fig. 9). The extremely fast establishment of the sorption equilibrium is a major advantage regarding the practical functionality of the present xerogel sorbents.

3.3. Desorption experiments

The xerogel pellets equilibrated with Ag(I) in batch sorption experiments were washed with different solutions to investigate the reversibility of the binding of Ag(I). Desorption is negligible when the pellet is washed with 5.0 mM EDTA solution in a single washing step. Washing the xerogel pellets with 5 mM NH_3 solution resulted in the dissolution of the xerogel. The efficiency of 10.0 mM $Na_2S_2O_3$ solution to regenerate the xerogel pellets was tested as a function of pH. At pH = 5 and 6, 80 and 90 % of the sorbed Ag(I) was recovered, respectively. As seen in Fig. 10, the complete recovery (98–102 %) of Ag(I) was achieved by

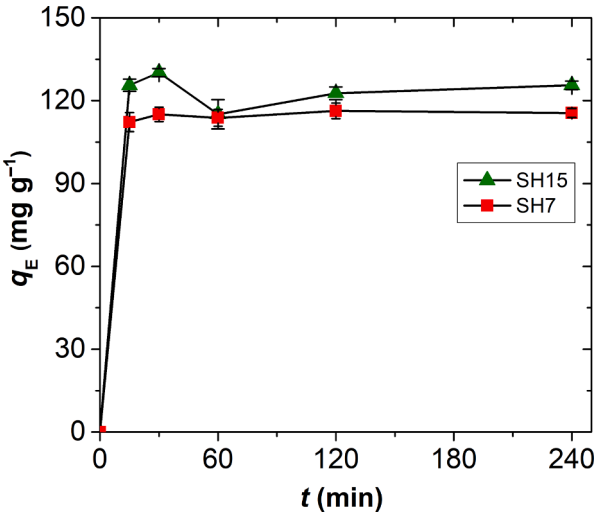

Fig. 9. The rate of the binding of Ag(I) on the functionalized xerogels. The *x*-axis shows the total contact time, which is the sum of the agitation time and the centrifugation time. (c_0Ag(I) = 50 mg L^{-1}; c_{Xgel} = 320 mg L^{-1}; pH = 5.0; T = 25 °C).

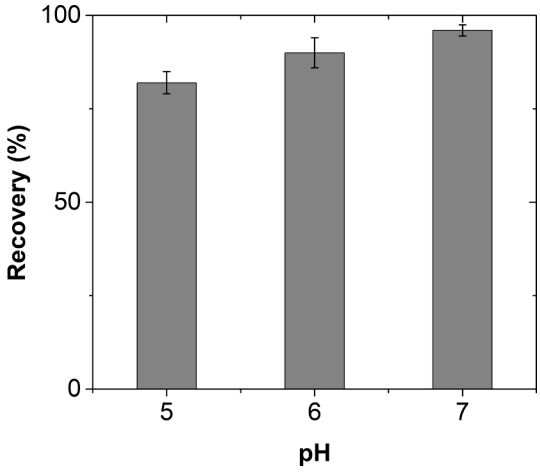

Fig. 10. Regeneration of SH7 by 10 mM $Na_2S_2O_3$ after equilibrating with aqueous Ag(I) as a function of pH. (c_0Ag(I) = 50 mg L^{-1}; c_{Xgel} = 320 mg L^{-1}; T = 25 °C).

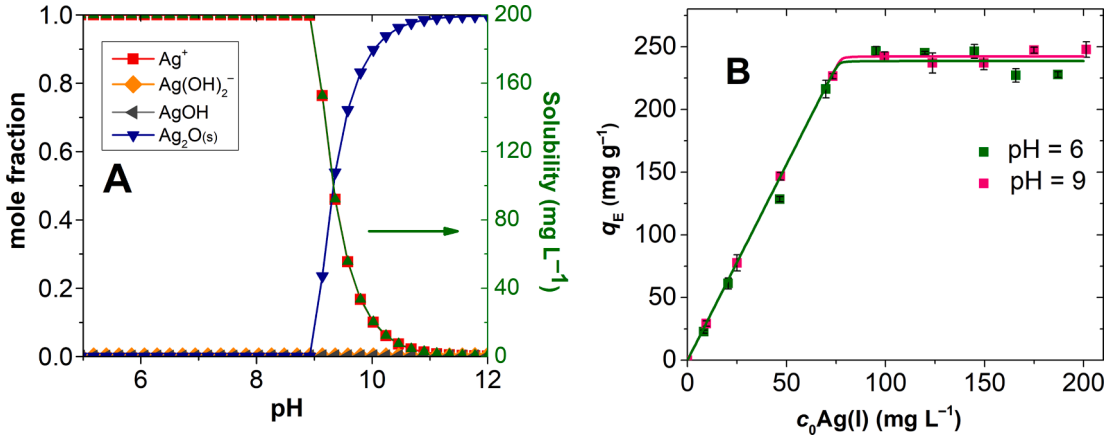

Fig. 8. Panel A: The speciation and the solubility of aqueous Ag(I) as a function of pH. Panel B: Sorption isotherms of Ag(I) on SH15 at pH = 5.0 (green symbols) and 9.0 (pink symbols) (c_{Xgel} = 320 mg L^{-1}; c_0Ag(I) = 10–200 mg L^{-1}; T = 25 °C). (For interpretation of the references to colour in this figure legend, the reader is referred to the web version of this article.)

washing the equilibrated xerogel pellet with 10.0 mM $Na_2S_2O_3$ solution at pH = 7.0. These results also demonstrate that the binding of Ag(I) is reversible, and the metal ions are not reduced on the surface of the xerogel.

The recycling of the xerogel sorbent was tested by performing consecutive sorption-regeneration cycles. The xerogel retained 91 ± 4 % of its sorption capacity after 3 cycles of regeneration.

3.4. Mechanism of sorption of Ag(I)

3.4.1. XPS and EDX analyses

The EDX analysis of the xerogels clearly shows that the as-prepared sample does not contain Ag, and the dominant elements are Si, O and C in the spectra. The lines of sulfur are very weak and hard to distinguish from the background. Following the sorption of aqueous Ag(I) by SH15, the characteristic lines of Ag, as well as, those of S appeared, which confirmed the existence of both elements in the equilibrated xerogels. Backscattered electron images revealed the presence of high atomic number elements in the spherical nanoparticles of the equilibrated xerogels. These areas have been scanned and EDX maps were generated, which also confirmed the saturation of the functionalized xerogel with Ag (Fig. 11).

XPS measurements were performed on the SH15 xerogel in its pristine form and after equilibrating with aqueous Ag(I) with the intent of exploring the chemistry of the binding by determining the chemical states of Ag and S. The survey XPS spectra confirmed the presence of silver in the respective sample (Fig. 12). However, a surprising finding was the apparent absence of sulfur. The peak fitting of the high-resolution Ag 3d spectrum confirms that the silver is present in of a single chemical state. The Ag 3d5/2 peak has a binding energy of 368.44 eV, which corresponds to Ag(I) most probably in the form of an oxide [43]. This is in good accordance with the results discussed in Section 3.3, namely that NH_3 and $Na_2S_2O_3$ solutions can quantitatively re-solubilize Ag(I) from the sorbents.

The lack of the detection of sulfur is explained by the limitations of the technique. XPS only yields information on the outermost few nanometers of any given material, and therefore, likely unable to obtain information from inside the pores. Ar^+-sputtering was attempted to expose the materials inside the pores, but no significant change was observed in the spectrum. Additionally, sulfur compounds may degrade when exposed to X-rays. Wang et al. used a monochromatic X-ray source in scanning mode to obtain structural information on sulfur-containing sorbents, and still reported technical difficulties [44].

3.4.2. Surface induced cluster formation of Ag(I)

The most probable explanation for the strong and selective binding of Ag(I) to the functionalized xerogels is the unique ability of this metal ion to form multinuclear (polymeric) complexes with alkyl thiol ligands [45,46]. Depending on the structure and the length of the side chains of the ligands, the formation of cyclic coordination compounds containing 4–11 Ag(I) centers were reported in the solution phase [45–48]. When precipitates form in the reaction of solvated Ag(I) and thiols, layered structures with long-range order were identified using X-ray crystallography [48,49]. The stability of these coordination compounds are reported to be exceptionally high, and the coordination of Ag(I) is favored even when the –SH group of the solvated ligand is still protonated [45–47]. Such high stability polymeric thiolate complexes do not exist in the case of any other metal ions, including Hg(II), despite their high affinity to sulfur compounds. The formation of mononuclear complexes is dominant in the case of the other soft metal ions, e.g. for aqueous Hg(II) and Pd(II).

Based on the literature reports and the present experimental data, we propose that a layered coordination compound forms from Ag(I) inside the mesopores of the functionalized xerogels, where the coordination of the silver atoms to the sulfur atoms follows a long range order, as depicted in Scheme 1. The exceptional stability of the Ag(I) coordination in the somewhat ordered pores is shown by the quasi stoichiometric binding of Ag(I) by the xerogels and the very high values of the fitted Langmuir equilibrium constants (cf. Fig. 7 and Table 3). The reduction of Ag(I) on the surfaces is ruled out by the demonstrated reversibility of the binding (cf. Section 3.3), and by the XPS result. The formation of this type of coordination compound on the surfaces of the functionalized mesoporous silicas also accounts for the observed trend of the linear increase of the sorption capacity with the thiol functionality of the xerogels. Until the silica surface is completely decorated by thiol groups, the decrease of the apparent surface area does not affect the coordination of Ag(I). All of these considerations point out that this specific surface complexation of Ag(I) is the reason for the high selectivity of the

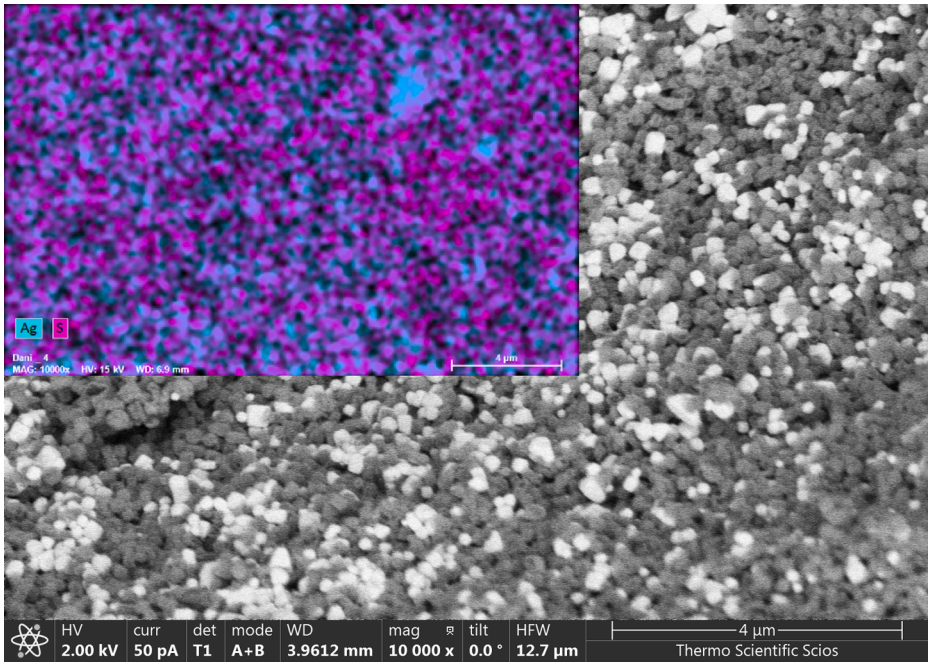

Fig. 11. Backscattered electron (BSE) SEM image and EDX map (inset) of the SH15 xerogel equilibrated with aqueous Ag(I).

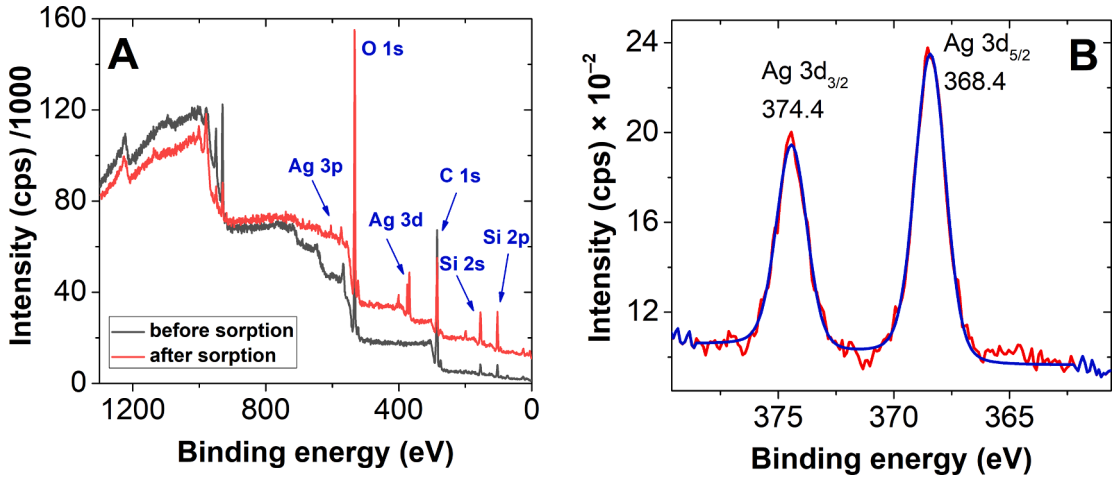

Fig. 12. Panel A: The XPS survey spectra of the SH15 xerogel before (black) and after (red) Ag(I) sorption. Panel B: High-resolution XPS spectrum of the Ag 3d region in the SH15 xerogel sample equilibrated with aqueous Ag(I). (For interpretation of the references to colour in this figure legend, the reader is referred to the web version of this article.)

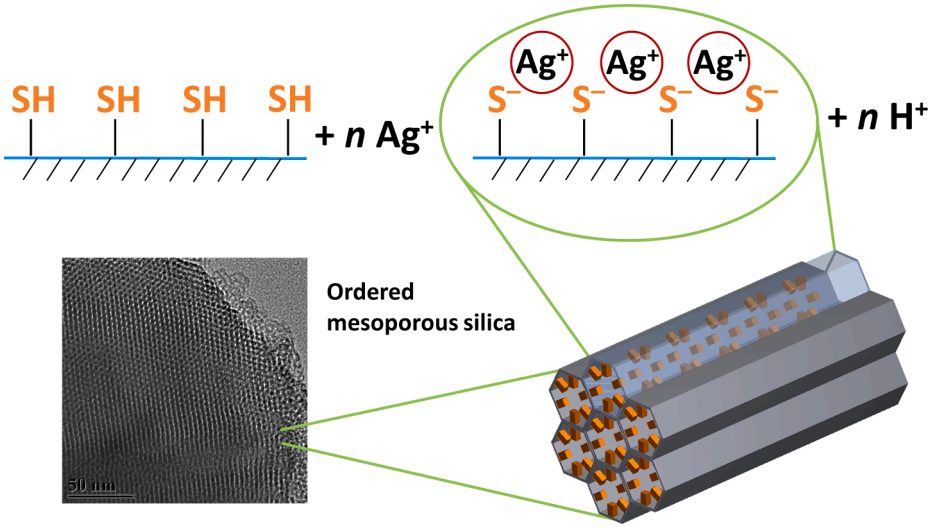

Scheme 1. The formation of the proposed long molecular range ordered layered structure of the Ag(I) coordination compound on the walls of the mesopores of the functionalized xerogels.

present functionalized quasi-ordered mesoporous silicas [50,51].

3.4.3. *Comparison with other sorbents*

There are relatively few sorbents developed for the selective binding of aqueous Ag(I) as compared to other toxic or valuable metal ions. The sorbents with the highest reported sorption capacities and having verified recovery of Ag(I) are collected in Table 4. In some cases, the selectivity is not discussed, which is a drawback for further development. When comparing the sorption capacities, no clear correlation can be established between the known preferential coordination modes of Ag(I) and the performance of the functionalized sorbents. Nevertheless, most of the previously reported sorbents have either lower sorption capacities or inferior selectivity than the functionalized mesoporous silicas of the present study. Another advantage of the presented family of xerogels is that the sorption of Ag(I) is completely reversible, no reduction takes place on the surface. This enables the practical and effective recovery of this precious metal ion and the regeneration of the sorbent.

4. Conclusions

The synthesis of thiol functionalized silica microparticles with an ordered porous structure has been achieved by the simplified co-condensation of TEOS with the thiol group containing silica precursor, MPTMS, using base catalysis and ambient conditions. Along with the increase of the number of the Ag(I)-binding thiol groups, the deterioration of the ordered pore structure and the decrease of the specific surface area were observed by XRD and N_2-sorption porosimetry. In spite of the latter effect, the increase of the thiol content resulted in the monotonous increase of the sorption capacity for Ag(I). The binding of aqueous Ag(I) is almost stoichiometric in a broad pH range even at low metal ion concentrations. The sorbent displays exceptionally high selectivity for Ag(I). The mechanism of binding of Ag(I) is proposed to be the reversible surface complexation in an ordered layered thiolate structure specific to this metal ion. This reversible complexation enables the practically complete recovery of Ag(I) and the regeneration of the sorbent. These properties make the reported functionalized mesoporous silicas attractive for the efficient recovery of Ag(I) even from realistic aqueous media where other dissolved metal compounds are abundantly present as technological byproducts.

Table 4
Comparison of the properties of effective Ag(I) sorbents. Examples are given only where the recovery of Ag(I) was verified experimentally.

Sorbent	Selectivity	Sorption capacity for Ag(I) (mg/g)	pH	ref.
Thiol functionalized mesoporous silica	Ag(I) (tested for 11 metal ions)	238	5.0–9.0	this work
Aminopropyl-functionalized mesoporous silica	Ag(I) (tested for 10 metal ions)	143	8.5	[11]
Chitosan / Montmorillonite Composite Beads	n./a.	43	6.0	[2]
Thiourea-modified chitosan resin	Ag(I) (tested for 9 metal ions)	407	4.0	[14]
Silica-coated magnetic nanoparticles	Au(III), Pd (II), Ag(I)	311	5.0	[24]
MCM-48 mesoporous silica functionalized with dendrimer amines	Ag(I) (tested for 8 metal ions)	169	5.0	[13]
Surface molecular-imprinted biosorbent	n./a.	199	7.0	[12]

CRediT authorship contribution statement

Petra Herman: Methodology, Validation, Formal analysis, Data curation, Conceptualization, Investigation, Writing – original draft, Visualization. **Dániel Pércsi:** Methodology, Validation, Formal analysis, Investigation. **Tamás Fodor:** Methodology, Validation, Formal analysis, Investigation. **Laura Juhász:** Methodology, Validation, Formal analysis. **Zoltán Dudás:** Methodology, Validation, Formal analysis, Investigation. **Zsolt Endre Horváth:** Methodology, Validation, Formal analysis. **Vasyl Ryukhtin:** Methodology, Validation, Formal analysis. **Ana-Maria Putz:** Conceptualization, Validation, Formal analysis, Data curation, Investigation, Supervision. **József Kalmár:** Methodology, Validation, Formal analysis, Data curation, Conceptualization, Resources, Writing – original draft, Writing – review & editing, Supervision. **László Almásy:** Methodology, Validation, Formal analysis, Conceptualization, Resources, Writing – original draft.

Declaration of Competing Interest

The authors declare that they have no known competing financial interests or personal relationships that could have appeared to influence the work reported in this paper.

Data availability

Data will be made available on request.

Acknowledgments

The research has been financially supported by the 2019-2.1.7-ERANET-2021-00021 project financed by the National Research, Development and Innovation Fund of the Ministry for Innovation and Technology, Hungary. The authors thank the Romanian Academy and the Inter-Academic Exchange Program between the Romanian Academy and the Hungarian Academy of Sciences.

Appendix A. Supplementary material

Additional experimental details and results of the SANS measurements referred to in the text. Supplementary data to this article can be found online at https://doi.org/10.1016/j.molliq.2023.122598.

References

[1] A. Sarı, M. Tüzen, Microporous Mesoporous Mater. 170 (2013) 155.
[2] T. Jintakosol, W. Nitayaphat, Mater. Res. 19 (2016) 1114.
[3] A. Bianchini, M. Grosell, S.M. Gregory, C.M. Wood, Environ. Sci. Tech. 36 (2002) 1763.
[4] M.J. Eckelman, T.E. Graedel, Environ. Sci. Tech. 41 (2007) 6283.
[5] H.T. Ratte, Environ. Toxicol. Chem. 18 (1999) 89.
[6] X. Song, P. Gunawan, R. Jiang, S.S. Leong, K. Wang, R. Xu, J. Hazard. Mater. 194 (2011) 162.
[7] M. Iqbal, A. Saeed, S.I. Zafar, J. Hazard. Mater. 164 (2009) 161.
[8] R. Waqar, M. Kaleem, J. Iqbal, L.A. Minhas, M. Haris, W. Chalgham, A. Ahmad, A. S. Mumtaz, Sustainability 15 (2023) 6024.
[9] A.R. Ladhe, P. Frailie, D. Hua, M. Darsillo, D. Bhattacharyya, J. Memb. Sci. 326 (2009) 460.
[10] M.J. Manos, C.D. Malliakas, M.G. Kanatzidis, Eur. J. Chem. 13 (2007) 51.
[11] H. Ebrahimzadeh, N. Shekari, N. Tavassoli, M.M. Amini, M. Adineh, O. Sadeghi, Microchim. Acta 170 (2010) 171.
[12] H.Y. Huo, H.J. Su, T.W. Tan, Chem. Eng. J. 150 (2009) 139.
[13] R. Taheri, N. Bahramifar, M.R. Zarghami, H. Javadian, Z. Mehraban, Powder Technol. 321 (2017) 44.
[14] L. Wang, R. Xing, S. Liu, H. Yu, Y. Qin, K. Li, J. Feng, R. Li, P. Li, J. Hazard. Mater. 180 (2010) 577.
[15] J. Aguado, J.M. Arsuaga, A. Arencibia, M. Lindo, V. Gascon, J. Hazard. Mater. 163 (2009) 213.
[16] N. Fellenz, F.J. Perez-Alonso, P.P. Martin, J.L. Garcia-Fierro, J.F. Bengoa, S. G. Marchetti, S. Rojas, Micropor. Mesopor. Mat. 239 (2017) 138.
[17] H. Javadian, M. Taghavi, Appl. Surf. Sci. 289 (2014) 487.
[18] F. Raji, M. Pakizeh, Appl. Surf. Sci. 282 (2013) 415.
[19] H.B. Garud, S.A. Jadhav, S.P. Jadhav, P.S. Suryawanshi, V.A. Kalantre, S. H. Burungale, S.D. Delekar, P.S. Patil, SILICON (2023).
[20] S.M. Mane, C.J. Raorane, J.C. Shin, Nanomaterials 12 (2022) 3232.
[21] A.-M. Putz, M. Ciopec, A. Negrea, O. Grad, C. Ianăşi, O.I. Ivankov, M. Milanović, I. Stijepović, L. Almásy, Materials 14 (2021) 628.
[22] D. Kumar, K. Schumacher, C.D.F. von Hohenesche, M. Grun, K.K. Unger, Colloids Surf. A 187 (2001) 109.
[23] P. Selvam, S.K. Bhatia, C.G. Sonwane, Ind. Eng. Chem. Res. 40 (2001) 3237.
[24] H. Vojoudi, A. Badiei, A. Banaei, S. Bahar, S. Karimi, G. Mohammadi Ziarani, M. R. Ganjali, Microchim. Acta 184 (2017) 3859.
[25] C. Ianăşi, P. Ianăşi, A. Negrea, M. Ciopec, O.I. Ivankov, A.I. Kuklin, L. Almásy, A.-M. Putz, Korean J. Chem. Eng. 38 (2021) 292.
[26] C. Ianăşi, E.-M. Picioruş, R. Nicola, A.-M. Putz, A. Negrea, M. Ciopec, A. Len, L. Almásy, Soft Mater. 20 (2022) S68.
[27] R. Nicola, O. Costisor, M. Ciopec, A. Negrea, R. Lazau, C. Ianăşi, E.M. Piciorus, A. Len, L. Almásy, E.I. Szerb, A.-M. Putz, Appl. Sci. 10 (2020) 2726.
[28] A.-M. Putz, O.I. Ivankov, A.I. Kuklin, V. Ryukhtin, C. Ianăşi, M. Ciopec, A. Negrea, L. Trif, Z.E. Horváth, L. Almásy, Gels 8 (2022) 443.
[29] A. Borówka, Ceram. Int. 45 (2019) 4631.
[30] A.-M. Putz, K.Z. Wang, A. Len, J. Plocek, P. Bezdicka, G.P. Kopitsa, T.V. Khamova, C. Ianăşi, L. Sacarescu, Z. Mitróová, C. Savii, M.H. Yan, L. Almásy, Appl. Surf. Sci. 424 (2017) 275.
[31] A.-M. Putz, L. Almásy, A. Len, C. Ianăşi, Fullerenes Nanotubes Carbon Nanostruct. 27 (2019) 323.
[32] P. Strunz, J. Saroun, P. Mikula, P. Lukas, F. Eichhorn, J. Appl. Cryst. 30 (1997) 844.
[33] M. Thommes, K. Kaneko, A.V. Neimark, J.P. Olivier, F. Rodriguez-Reinoso, J. Rouquerol, K.S.W. Sing, Pure Appl. Chem. 87 (2015) 1051.
[34] Z. Dudás, A. Len, C. Ianăşi, G. Paladini, Mater. Charact. 167 (2020), 110519.
[35] C.J. Brinker, T.L. Ward, R. Sehgal, N.K. Raman, S.L. Hietala, D.M. Smith, D.W. Hua, T.J. Headley, J. Membr. Sci. 77 (1993) 165.
[36] R.F.S. Lenza, W.L. Vasconcelos, Mater. Res. 4 (2001) 189.
[37] J.M. Berquier, L. Teyssedre, C. Jacquiod, J. Sol-Gel Sci. Technol. 13 (1998) 739.
[38] M. Mihelčić, A.K. Surca, A. Kreta, M. Gaberšček, Croat. Chem. Acta 90 (2017) 169.
[39] S. Bandyopadhyay, A. Dey, Analyst 139 (2014) 2118.
[40] Y.S. Li, Y. Wang, T. Tran, A. Perkins, Spectrochim. Acta A: Mol. Biomol. Spectrosc. 61 (2005) 3032.
[41] G.V. Franks, J. Colloid Interface Sci. 249 (2002) 44.
[42] Chem. Int. – Newsmagazine for IUPAC 28 (2006) 26.
[43] M. Romand, M. Roubin, J.P. Deloume, J. Electron Spectrosc. Relat. Phenom. 13 (1978) 229.
[44] B. Wang, K. Wu, T. Liu, Z. Cheng, Y. Liu, Y. Liu, Y. Niu, J. Hazard. Mater. 442 (2023), 130121.
[45] R.A. Bell, J.R. Kramer, Environ. Toxicol. Chem. 18 (1999) 9.
[46] B. Krebs, G. Henkel, Angew. Chem. Int. Ed. 30 (1991) 769.
[47] I.G. Dance, K.J. Fisher, R.M.H. Banda, M.L. Scudder, Inorg. Chem. 30 (1991) 183.
[48] I.G. Dance, L.J. Fitzpatrick, A.D. Rae, M.L. Scudder, Inorg. Chem. 22 (1983) 3785.
[49] K. Tang, M. Aslam, E. Block, T. Nicholson, J. Zubieta, Inorg. Chem. 26 (1987) 1488.
[50] Y. Zhang, D. Liu, W. Guo, Y. Ding, J. Mol. Liq. 372 (2023), 121229.
[51] J. Song, X. Cao, Z. Huang, J. Mol. Liq. 367 (2022), 120428.